J. Fluid Mech. (2001), *vol.* 446, *pp.* 253–269.
DOI: 10.1017/S0022112001005699 Printed in the United Kingdom

Buoyancy-driven interactions of viscous drops with deforming interfaces

By JOSEPH KUSHNER IV, MICHAEL A. ROTHER AND ROBERT H. DAVIS†

Department of Chemical Engineering, University of Colorado, Boulder, CO 80309–0424, USA

(Received 31 May 2000 and in revised form 21 January 2001)

Experiments were conducted on the interactions of two different-sized deformable drops moving due to gravity in an immiscible viscous fluid at low Reynolds number. As the drops come close to each other, several interactions are possible: (i) separation of the drops, (ii) capture of the smaller drop behind the larger drop, (iii) breakup of the smaller drop into two or more drops, and (iv) pass-through of one drop through the other, with possible cycle interaction or leap-frogging. The interactions depend on several system parameters, including the drop-to-medium viscosity ratio, the radius ratio of the two drops, the initial horizontal offset of the two drops at large vertical separation, and the gravitational Bond number (which represents the ratio of buoyant forces to interfacial tension forces for the larger drop and describes how much the drops will deform). Experimental analysis was conducted by videotaping trajectories of glycerol–water drops of various compositions falling in castor oil. The results show good agreement with available theoretical results, both for interaction maps and individual trajectories. The results also provide data beyond the present limitations of theoretical algorithms and reveal the new pass-through phenomenon.

1. Introduction

The study of deformable drops in low Reynolds number flow is applicable to emulsion sedimentation and creaming, polymer blending, liquid–liquid extraction, and magma interactions. For linear flows, there have been several recent experimental works (Guido & Simeone 1998; Tretheway, Muraoka & Leal 1999; Hu, Pine & Leal 2000) on two colliding drops which examined the effects of small deformation on coalescence. Also, for selected physical systems in thermocapillary motion, pairwise interactions of bubbles (Wei & Subramanian 1994) and drops (Nallani & Subramanian 1993) have been studied to describe the hydrodynamics. We also note the extensive literature concerning high-speed collisions of drops (e.g. Qian & Law 1997; Orme 1997; Ashgriz & Poo 1990; Menchaca-Rocha *et al.* 1997).

Nonetheless, for the case of two drops or bubbles in buoyancy motion at low Reynolds number, experimental investigations have been limited. Of relevance here are studies on slightly deformable drops (Zhang, Davis & Ruth 1993), on the behaviour of pairs of drops made from dilute dispersions of microscopic particles in the absence of interfacial tension (Machu *et al.* 2001), and on the enhanced coalescence phenomena observed with highly deformable air bubbles rising in corn syrup (Manga & Stone 1993, 1995). Although it has been demonstrated (Yiantsios & Davis, 1990, 1991) that

† Author to whom correspondence should be addressed: robert.davis@colorado.edu

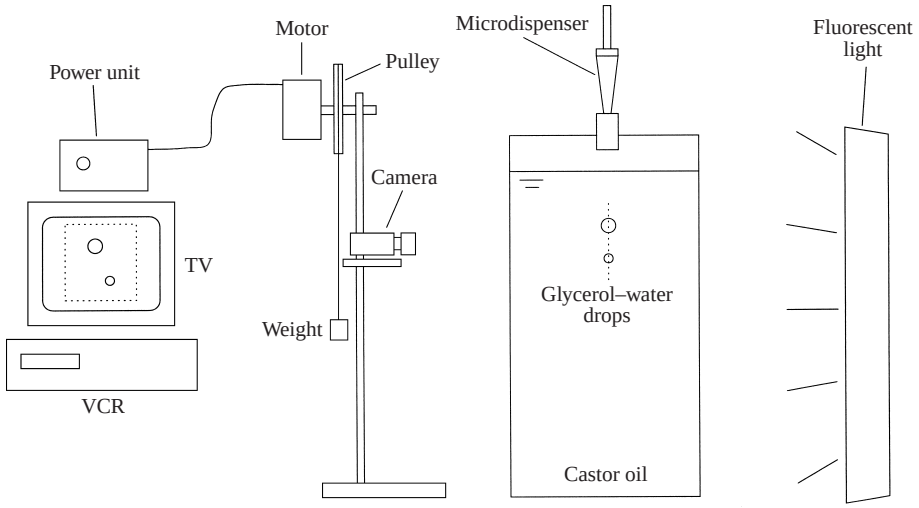

FIGURE 1. Sketch of the experimental setup for buoyancy-driven motion of deformable drops.

small deformation inhibits coalescence due to the slower film drainage, Manga & Stone (1993, 1995) showed that moderate deformations cause two drops to align and may result in enhanced coalescence rates. Using boundary-integral methods, related calculations by Zinchenko, Rother & Davis (1997, 1999) and Davis (1999) show that the drop-to-medium viscosity ratio is crucial to the outcome of two-drop interactions. At viscosity ratios close to zero, as in the case of bubbles, alignment and enhanced coalescence take place. In contrast, at viscosity ratios close to unity, breakup of the smaller trailing drop is possible, as are more complicated interactions.

By using a mixture of glycerol and water for the drop phase to control the viscosity ratio relative to a castor-oil medium, the experiments described here were performed to evaluate the theoretical findings and move beyond the limitations of the simulations to provide a more comprehensive picture of the possible behaviours. The details of the experimental procedures are provided in § 2. Then, in § 3, experimental results and comparison with theory are presented. Concluding remarks make up the final section, § 4.

2. Materials and methods

The experimental apparatus, which is similar to those used previously for slightly deformable drops (Zhang *et al.* 1993) and highly deformable bubbles (Manga & Stone 1993, 1995), is shown in figure 1. Made of 3/4 in. Plexiglas, the tank is 40 cm × 40 cm in the horizontal plane, with a height of 120 cm. A Pulnix 7-CN CCD camera is mounted on a motor-driven stand, so that the drops remain in the image as they fall. The interactions are then recorded on a Sony SLV-400 VCR, viewed on a Sony SSM-125 monitor, and analysed. For a few experiments, still photographs were taken for illustrative purposes at successive times with an Olympus OM-1 35 mm camera. To illuminate the drops, the tank was lit from behind by two Phillips 34 W fluorescent light bulbs.

The drop sizes are controlled (typically to within $\pm 2\%$ by diameter) by two Gilson Pipetman microdispensers with capacity 1000 µl. For drops larger than 1 ml, a Pipet-aid (Drummond Scientific, Serial No. D 33943) and 10 ml Fisherbrand plastic serological pipets (Fisher Scientific, Catalog No. 13-676-10s) were used to deliver the

System	wt. % H_2O	μ'/μ_e ($g\,cm^{-1}\,s^{-1}$)	ρ'/ρ_e ($g\,cm^{-3}$)	σ ($dyn\,cm^{-1}$)	T (°C)
1	75	0.0184/8.67	1.06/0.948	20	23
2	16	0.748/7.73	1.21/0.948	13	24
3	1.6	7.53/7.73	1.24/0.948	12	24

TABLE 1. Properties of three glycerol–water/castor oil systems used in experiments.

drops. The smaller drop is introduced first and allowed to settle at least 8–10 cm before the second, larger drop is introduced which catches up and interacts with the first drop. Drop radii were varied in the range 0.15–0.83 cm, with the corresponding Reynolds numbers (based on the radius and isolated velocity of the larger drop) in the range 0.008–0.4. Two pipet holders, whose position can be controlled by clamps along a horizontal bar, determine the horizontal offset between the drops. The experiments were performed at room temperature (23–24 °C), and the fluid temperature was typically measured to within 0.2 °C prior to each experiment. When each videotape was reviewed, it was verified visually that the plane of motion was perpendicular to the camera.

By varying the amount of water mixed with glycerol to make the drops, the drop-to-medium viscosity ratio can be changed from 0.001 to 1.5. For the results discussed below, three drop compositions were used: 1.6%, 16% and 75%, where the percentage is that of water by weight. Castor oil served as the viscous, suspending liquid. In table 1, the physical properties of the three systems at their nominal temperatures are listed, where μ' and ρ' are the viscosity and density of the drop phase, μ_e and ρ_e are those of the matrix, and σ is the interfacial tension. Density measurements were conducted by weighing a known volume on a Mettler AE100 electronic mass balance. Viscosity measurements were made with Cannon Fenske Routine Viscometers (N745, size 450; KIMAX, No. 46460, H33, size 150). For each solution tested, six timed viscosity runs were conducted, and the results were averaged to obtain the value of the viscosity at the recorded temperature. The measured values of ρ' and μ' are in good agreement with handbook values (Mellan 1970).

The interfacial tension σ was measured by a pendant drop apparatus using the procedure outlined in Ambwani & Fort (1979). The data indicate that the interfacial tension increases linearly with water content according to the best fit

$$\sigma = 0.107x + 11.8, \tag{1}$$

where σ has units $dyn\,cm^{-1}$ and x is weight % H_2O.

3. Results and discussion

3.1. *Isolated drop velocities*

Figure 2 presents single drop velocities, V_{exp}, made dimensionless by the Stokes settling velocity, V_{St}, of a rigid sphere:

$$V_{St} = \frac{2(\rho' - \rho_e)ga^2}{9\mu_e}, \tag{2}$$

where a is the undeformed drop radius and g is the gravitational acceleration. The dashed line connects the experimental values, where the error bars are plus and minus

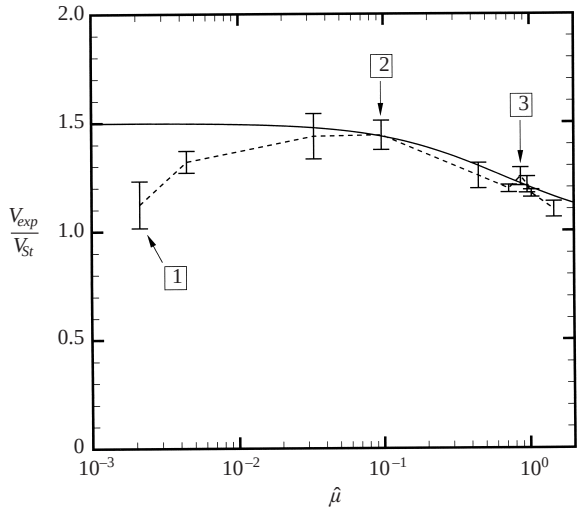

FIGURE 2. Isolated drop velocities V_{exp} made dimensionless by the Stokes settling velocity V_{St} as a function of viscosity ratio $\hat{\mu}$. The dashed line joins the experimental values, which are shown as plus-and-minus one standard deviation from the mean, and the solid line is the theoretical curve. The three systems of table 1 are identified.

one standard deviation from the mean. The solid line is the theoretical curve for the velocity of an isolated drop provided by the Hadamard–Rybczynski formula:

$$\frac{V^{(0)}}{V_{St}} = \frac{(\hat{\mu}+1)}{(\hat{\mu}+2/3)}, \tag{3}$$

where $\hat{\mu} = \mu'/\mu_e$ is the drop-to-medium viscosity ratio. The Reynolds number for figure 2 is in the range 0.008–0.2, as a broad range of drop sizes was used. Theory and experiment are in good agreement for $\hat{\mu} \geqslant 0.03$. Surfactant contamination in the water is a possible explanation for the rigid-interface behaviour observed at low $\hat{\mu}$ (high weight % H_2O). Further discussion of sources of experimental error is given in § 3.2 below.

3.2. *Characteristic interactions of two glycerol–water drops*

The parameter space for two-drop interactions was investigated for the three systems in table 1. Several different types of interactions were observed, which can be broken down into four basic categories: separation, capture, breakup, and pass-through. These interactions depend on the viscosity ratio, $\hat{\mu} = \mu'/\mu_e$, the size ratio, $k = a_1/a_2 < 1$ (the subscript 1 refers to the smaller drop, while 2 is for the larger drop), the initial dimensionless horizontal offset (at large vertical offset), $\Delta x_0/a_2$, and the gravitational Bond number:

$$Bo = (\rho' - \rho_e)ga_2^2/\sigma. \tag{4}$$

Two spherical drops may coalesce in the absence of any attractive force due to an integrable singularity in the hydrodynamic resistance (Zinchenko 1982; Davis, Schonberg & Rallison 1989; Zhang & Davis 1991), while small but finite deformation prevents contact in a finite time (Yiantsios & Davis 1990, 1991). However, macroscopic deformation of the drop or bubble interfaces causes changes in the velocities that result in alignment and possible capture or entrainment events (Manga & Stone 1993, 1995). At low viscosity ratios ($\hat{\mu} \ll 1$), coalescence is promoted by the interfacial

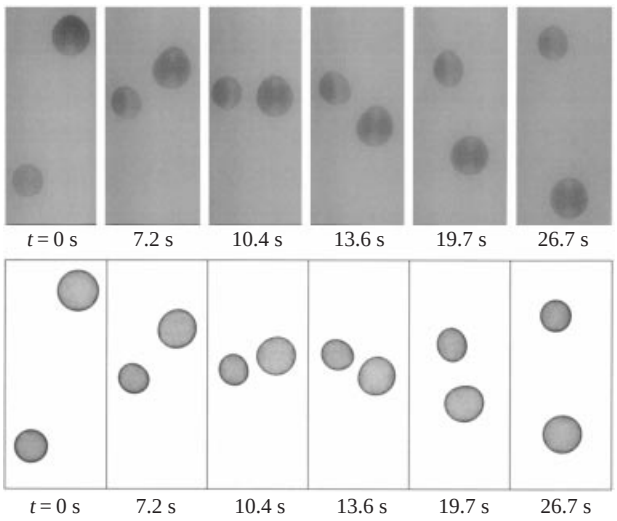

FIGURE 3. Experimental images and theoretic predictions of the drop shapes for Run 1 (see table 2), a trajectory leading to separation.

shape variations (Manga & Stone 1993, 1995), but when $\hat{\mu} = O(1)$, the trailing smaller drop may experience sufficient viscous drag in the extensional flow behind the larger one to induce breakup (Zinchenko *et al.* 1997, 1999; Cristini, Blawzdziewicz & Loewenberg 1998; Davis 1999). More exotic behaviours have also been observed in boundary-integral simulations (Zinchenko *et al.* 1999; Davis 1999) and experiments (Machu *et al.* 2001).

Separation

An example of separation interaction is illustrated in figure 3. Separation between two deformable drops will occur at values of $\Delta x_0/a_2$ above a critical value of the offset for each Bond number, as well as below some critical Bond number where only separation occurs for any value of $\Delta x_0/a_2$. To keep presentation compact, the physical conditions for figure 3 and subsequent example interactions are summarized in table 2 by reference to run number. The Reynolds number in table 2 is defined as $Re = \rho_e V_2^{(0)} a_2/\mu_e$, where $V_2^{(0)}$ is the isolated velocity from (2) and (3) for drop 2. In figure 3, an experimental trajectory is shown for Run 1. The drops deform, but they separate after interacting. Below the experimental pictures, a series of boundary-integral simulations (using the code of Zinchenko *et al.* 1999) is presented at the same time instants as the experimental ones, demonstrating qualitative agreement but with the drops predicted to approach more closely and separate more slowly than observed experimentally, possibly due to surfactant effects.

Figure 4 is a graph of the centroid-to-centroid distance r made dimensionless by a_2 vs. the angle θ between vertical and the line of centroids for the experiment in figure 3. An additional trajectory with constant horizontal offset (no interaction) is shown as a dotted line for comparison. Again, it is seen that the drops did not move as close together as predicted by the boundary-integral simulation, and they subsequently moved apart more readily for $\theta > \pi/2$. The discrepancy may be due, in part, to surfactant contamination causing Marangoni stresses in this system of high water content. In addition, the viscosity of the castor oil varies by more than 10%

Run	System	k	$\hat{\mu}$	Bo	$\Delta x_0/a_2$	Re
1	1	0.81	0.002	1.8	2.0	0.090
2	2	0.77	0.1	5.8	2.3	0.17
3	1	0.80	0.002	0.71	0.15	0.021
4	3	0.66	1.0	5.6	0.70	0.11
5	3	0.87	1.0	7.1	1.6	0.16

TABLE 2. Parameters of experimental runs described in text.

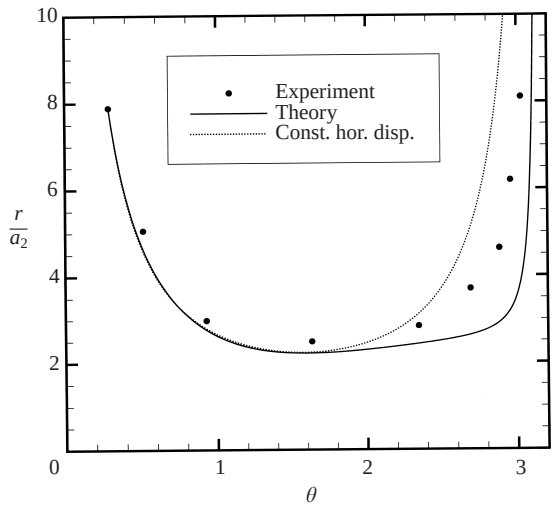

FIGURE 4. Experimental (solid circles) and theoretical (solid line) drop trajectories for separation under the same conditions as figure 3, shown as dimensionless centroid-to-centroid distance r/a_2 vs. the angle θ between vertical and the line of centres. The dotted line is a trajectory with constant horizontal displacement.

with a temperature change of 1 °C (see table 1), and so small temperature differences may noticeably affect the time scale.

Capture and coalescence

Run 2 (illustrated in figures 5 and 6) is an example of capture, when the smaller drop is passed by the faster-moving larger drop, entrained behind it, and then pulled into a dimple in the rear of the now leading larger drop. Possible tip streaming from the smaller drop was observed visually at times corresponding to those between frames 4 and 5 of figure 5, though the phenomenon is difficult to discern in the still photographs. A discussion of the likelihood of surfactant contamination with System 2 is found in the discussion of breakup and passthrough in § 3.3. Unambiguous evidence of tip streaming was seen in comparable capture runs with System 1. As described in the literature (de Bruijn 1993; Sherwood 1984), tip streaming occurs when a dilute surfactant accumulates and causes low interfacial tension close to the sharp ends of drops. Subsequently, the shear stresses exerted by the continuous phase pull out a stream of droplets from the tip. The computational results predict that a wedge-shaped cusp forms at the end of the trailing drop, and smoothing (Zinchenko *et al.* 1999) must be used to extend the simulation when the smaller drop is held

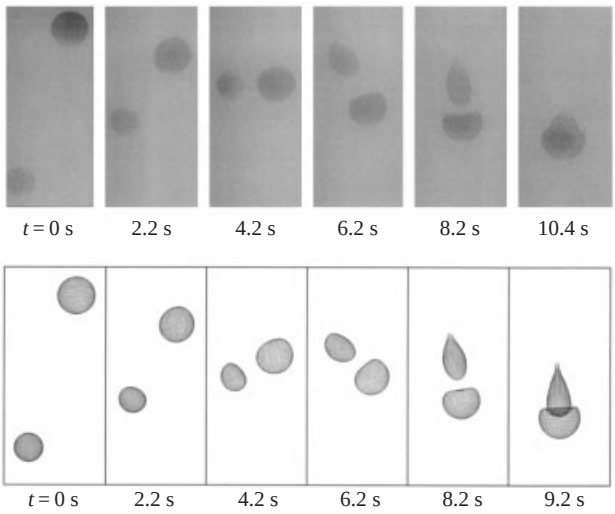

FIGURE 5. Experimental images and theoretical predictions of the drop shapes for Run 2 (see table 2), a trajectory leading to capture. The boundary-integral code cannot proceed beyond the last frame in the simulation.

inside the larger one. Even with smoothing, however, the boundary-integral results cannot proceed beyond $t = 9.2$ s for this case. Nevertheless, the simulations with smoothing are in good agreement with the experiments and indicate capture by a strong reduction in r/a_2 as $\theta \to \pi$ (see figure 6).

For the case of figure 5, coalescence was not observed before the pair reached the bottom of the tank. For smaller drops, however, film drainage from the gap is quicker due to a decreased region of deformation, and formation of a single drop after film rupture is often seen. In fact, coalescence was observed for all values of $\hat{\mu}$ at $k = 0.8$ in a small range of Bond numbers just above the critical value for capture in most cases. In the lower part of figure 6, a series of experimental images (captured from videotape for Run 3 in table 2) is shown just prior to, during, and after coalescence.

Breakup

The third basic category of interaction of two deformable drops is breakup, which is illustrated in figure 7 for Run 4 of table 2. In the experiments, the trailing drop stretches in the extensional flow behind the larger drop, before breaking into four daughter drops. In the simulation, the drops separated more rapidly than observed experimentally, and so the smaller drop does not become as extended and it pinches off sooner due to the weakening of the local extensional flow as it recedes from the larger drop.

Various modes of breakup of the smaller drop behind the larger drop were observed, depending on the system parameters. For size ratios close to unity and/or very large Bond numbers, the smaller drop became very long and then experienced a capillary-type breakup into numerous (50+, in some experiments) tiny drops. On the other hand, for smaller size ratios and Bond numbers only slightly greater than the critical value for breakup, the smaller drop remained more compact and broke into a few daughter drops of comparable size (as seen in figure 8); a similar behaviour was seen for small initial horizontal offsets. Finally, if the initial horizontal offset was just below the critical value (above which separation without breakup occurred), then a very small tail broke off from the relatively large head of the smaller drop.

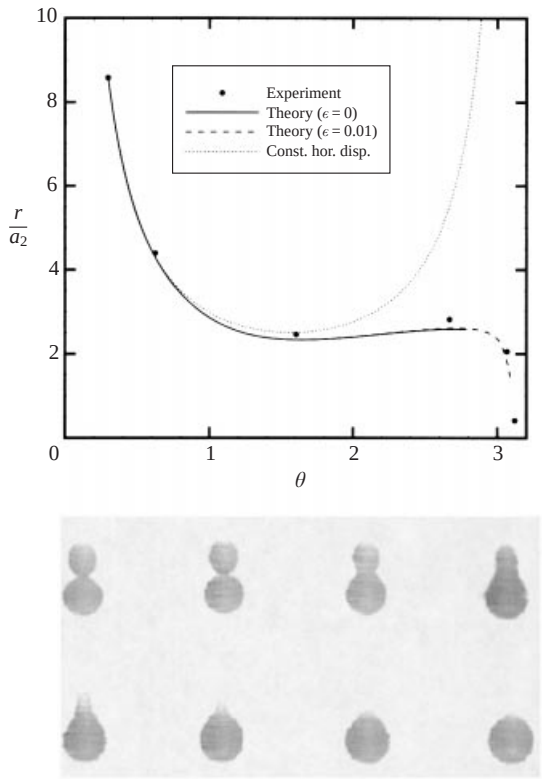

FIGURE 6. Experimental (solid circles) and theoretical drop trajectories for capture under the same conditions as figure 5, shown as dimensionless centroid-to-centroid distance r/a_2 vs. the angle θ between vertical and the line of centres. The solid line is theory for a conventional boundary-integral run, while the dashed line has some exponential smoothing to alleviate the cusp ($\epsilon = 0.01$, Zinchenko *et al.* 1999) and allow continuation until capture is evident. The dotted line is a trajectory with constant horizontal displacement. Below the graph are experimental images captured from video of Run 3 (see table 2) showing drop coalescence. The total time elapsed between the first and last images is about 4 s.

Pass-through

The fourth basic category of interactions observed is the new pass-through or leap-frog interaction, which is shown in figure 8 for Run 5 of table 2. This interaction occurs for cases of severe drop deformation, much like the breakup interaction. The distinction between when breakup and pass-through occur depends mostly on the horizontal separation of the two drops. At high Bond numbers, breakup will occur in a region near the critical offset or demarcation between separation and breakup, while pass-through occurs when the drops are closer together. The qualitative features of the experiment are evident, although the drops were observed to move together more quickly than predicted, possibly due to inertia effects and/or uncertainties in viscosity measurements.

From a comparison of figures 7 and 8, it can be seen that the pass-through interaction begins in a similar fashion to that of the breakup interaction, with the smaller drop moving to the rear of the larger drop and then stretching and breaking. The difference in the two interactions occurs because the drop that was formed from the head of smaller drop during breakup in figure 8 is still large enough to be

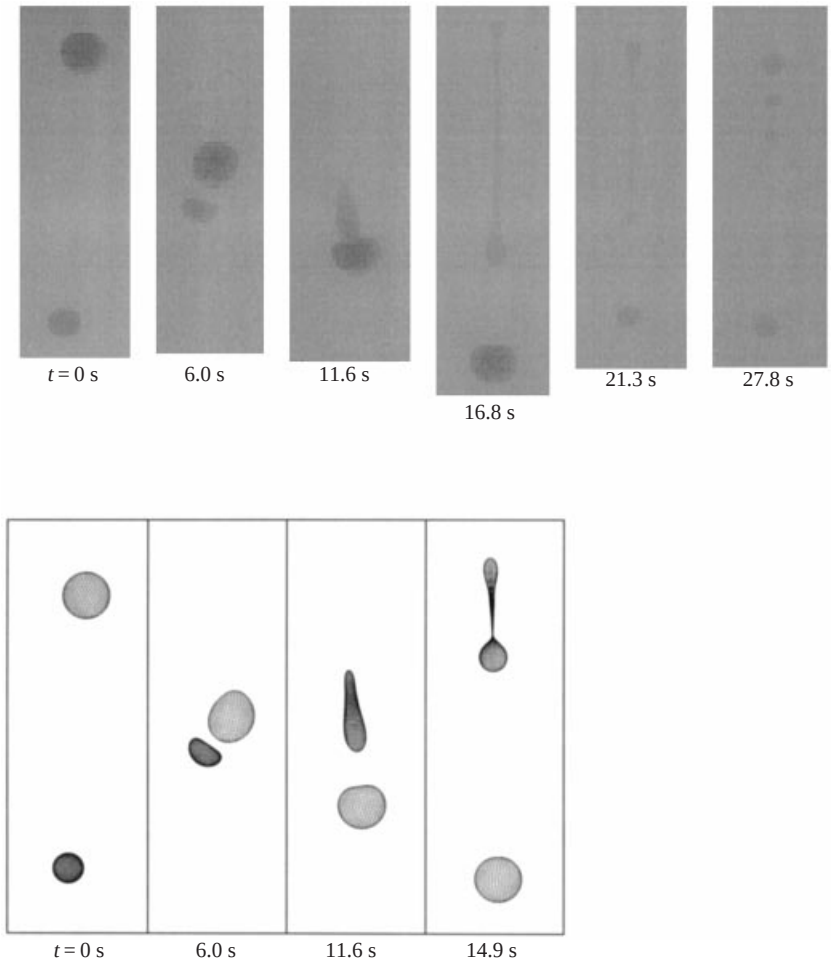

FIGURE 7. Experimental images and theoretical predictions of the drop shapes for Run 4 (see table 2), a trajectory leading to breakup. The boundary-integral code cannot proceed beyond the last frame shown in the simulation.

captured by the larger drop. However, due to the highly deformable nature of this new two-drop system, the smaller drop does not simply sit on top of the larger drop, but instead passes through a hole which forms in the centre of the larger drop. After it emerges at the front (bottom) of the larger drop, it passes around to the rear of the larger drop due to buoyancy and the difference in sizes, and the pass-through process may be repeated. In this case, the phenomenon is reminiscent of leap-frogging, such as has been simulated for two pairs of particles or drops in which the trailing pair moves faster and replaces the leading pair under appropriate configurations (Manga & Stone 1995; Hocking 1964; Durlofsky, Brady & Bossis 1987).

The pass-through or leap-frog phenomenon is too complex for the current three-dimensional boundary-integral simulations. However, the early stages of pass-through were simulated for axisymmetric Stokes motion by Davis (1999). He showed that a dimple forms on the rear of the leading drop and that, for viscosity ratio near unity, the dimple can form a plume which passes through the axis of the drop so that a torus is formed. At sufficiently high Bond numbers, the head of the trailing drop is

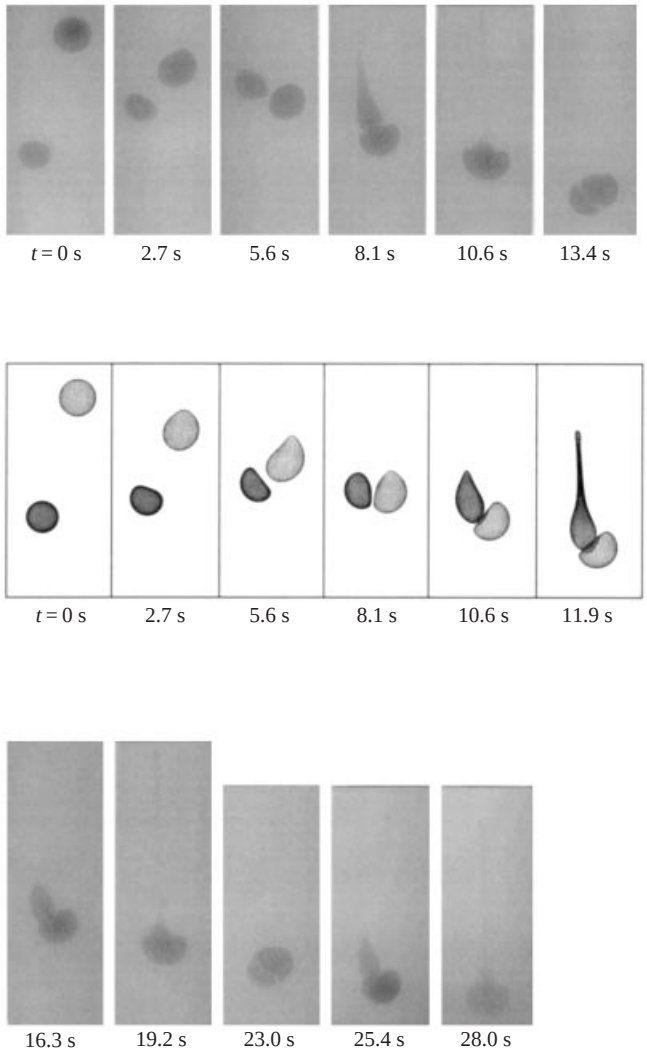

FIGURE 8. Experimental images and theoretical predictions of the drop shapes for Run 5 (see table 2), a trajectory leading to cyclic pass-through. The boundary-integral code cannot proceed beyond the last frame shown in the simulation.

sucked into this plume, although the code was not able to simulate breakthrough of the trailing drop and its emergence on the other side. In recent work with 'drops' formed by dilute clouds of small particles, Machu *et al.* (2001) also observed torus formation and the passage of the trailing drop into the centre of the leading drop, and they were able to simulate the motion by treating individual particles with Stokeslets. Related investigations of axisymmetric behaviour at higher Reynolds numbers have been reported in experiments on vortex rings formed by two drops (Baumann *et al.* 1992; Joseph & Renardy 1993). In their work, Joseph and coworkers describe how the membrane, which thins as a vortex ring forms from a drop, sometimes ruptures as another drop, or vortex ring passes through it, and they call the interaction 'poke-through'. Using vortex rings made visible by smoke, Yamada & Matsui (1978, 1979) have illustrated a 'mutual slip-through' interaction in which a trailing smoke ring

passes through a leading smoke ring, whereupon the process is repeated. Faber (1995) refers to this process as 'leap-frogging'.

In studies with single viscous drops, Kojima, Hinch & Acrivos (1984) showed that an infinitesimal indentation in the rear of a sedimenting drop will grow only in the limit of zero interfacial tension, while Koh & Leal (1989) and Pozrikidis (1990) showed that the dimple will grow to form a plume and convert the drop to a torus only if the initial deformation is sufficiently large for finite interfacial tension. For the interaction of two drops, the flow field created by the trailing drop causes the leading drop to flatten, initially into a prolate shape and then with a dimple at its rear. The recirculation pattern in the leading drop driven by the external flow represents a pumping action which causes the dimple to grow and, if the restoring interfacial tension forces are weak (high Bo), form a plume. Tiny air bubbles entrained in the drops for a few of our experiments confirmed the internal flow pattern which leads to dimple growth and plume formation.

There are several different variations in the pass-through interaction that can occur after the smaller drop passes through the larger one. If the two drops cleanly separate and are perfectly uniaxial, it is possible, though very rare, that the larger drop subsequently may be pulled through the smaller drop in a manner similar to the general pass-through interaction described above. Otherwise, the smaller drop will be forced to the side of the larger drop and then move around to its rear. If a large amount of material from the smaller drop was lost during its breakup in the initial pass-through interaction, the larger drop will then leave the smaller drop behind. However, if only a small amount of material was lost during the initial breakup, the smaller drop will be passed through the larger drop again, as shown in figure 8, so that leap-frogging occurs. While at most three complete leap-frog interaction cycles were observed in the experiments before the bottom of the tank was reached, leap-frogging will otherwise continue until the smaller drop has lost enough material by breakup that separation occurs or until the two drops coalesce during a pass-through interaction. In the limit of infinite Bond number or no interfacial tension, the two drops keep mixing together in the recirculating flow (Machu *et al.* 2001).

3.3. *Two-drop interaction maps*

Interaction maps are presented in this section. To study capture, System 1 was used for size ratios $k = 0.7$ and 0.8. To also study breakup and pass-through, Systems 2 and 3 were used with $k = 0.8$. In conducting these experiments, values of k with errors less than ± 0.015 from the target values were deemed acceptable for addition to the interaction maps. In all cases, the initial horizontal offsets were extrapolated to infinite vertical separation, using far-field mobility functions for spherical drops at large separations. Comparisons are made with the predictions from boundary-integral simulations by Zinchenko *et al.* (1999). These simulations also show that the initial vertical separation of at least 10 times the larger drop radius in the experiments is sufficient to determine the critical offset for infinite initial separation to within 3%.

Capture and coalescence

In figure 9, for System 1 with $\hat{\mu} = 0.002$ and $k = 0.7$, good agreement in the offsets is observed between theory and experiment for the critical Bo which delineates separation and capture. The open symbols are for experiments which ended in separation of the two drops, whereas the closed symbols are for experiments where capture occurred. The dashed line demarcates the experimental boundary between separation and capture, whereas the solid line is the corresponding prediction from

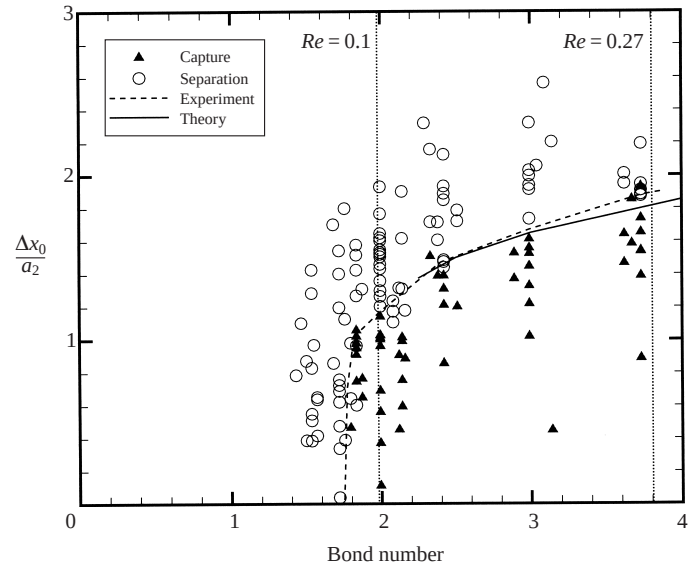

FIGURE 9. Interaction map for $\hat{\mu} = 0.002$ and $k = 0.7$. Filled symbols represent capture events, while hollow ones are for separation. The solid line marks theory (Zinchenko *et al.* 1999), with capture below the line and separation above the line, and the dashed line is a fit of the experiments.

Zinchenko *et al.* (1999). As expected, when the initial horizontal offset exceeds a critical value for a given Bond number, the drops do not come sufficiently close for capture to occur. Moreover, the critical offset increases with increasing Bo as the deformation-induced alignment becomes greater. The most striking though well-established (Manga & Stone 1993, 1995) feature in figure 9, and figure 10 below, is that the capture cross-section of very deformable drops and bubbles at low viscosity ratios can be much greater than that for spherical ones. At $Bo < 2.25$, no theory is yet available due to limitations of the present code for very small gaps, but an experimental turning point was found where the critical offset dropped to zero. Thus, for $Bo < 1.8$, no capture is seen. For $k = 0.7$, no coalescence was observed because, even at the smallest Bo where capture still occurs, the film drainage requires more time than it takes for the drops to fall the length of the tank.

In figure 10, for System 1 with $\hat{\mu} = 0.002$ and $k = 0.8$, there is also reasonable agreement in the critical offsets, though the agreement is not as good as in figure 9 for the larger values of Bo. The increased error could be due to more significant wall effects, as well as finite inertia, since the critical offsets are larger due to the increased size ratio. Limitations in the present boundary-integral algorithm prohibit critical offset determination below $Bo = 1.5$ for this case. Experimental results were obtained down to $Bo = 0.5$, yielding three interesting results. The first is a levelling off of the critical offset curve at a value of 1.8 for the dimensionless horizontal separation. The second is the complete end of all capture interactions below $Bo = 0.6$, which is much lower than observed in figure 9 for $k = 0.7$. The final result to note is the presence of the two separate regions of capture with and without coalescence. Simple capture (without coalescence by the time the bottom of the tank is reached) occurs for $Bo > 0.9$, while capture with coalescence occurs for $0.65 \leqslant Bo \leqslant 0.9$. It should be noted that the distinction between capture with and without coalescence is one due solely to the finite size of the tank.

Both the isolated drop velocities and the presence of tip streaming seem to indicate

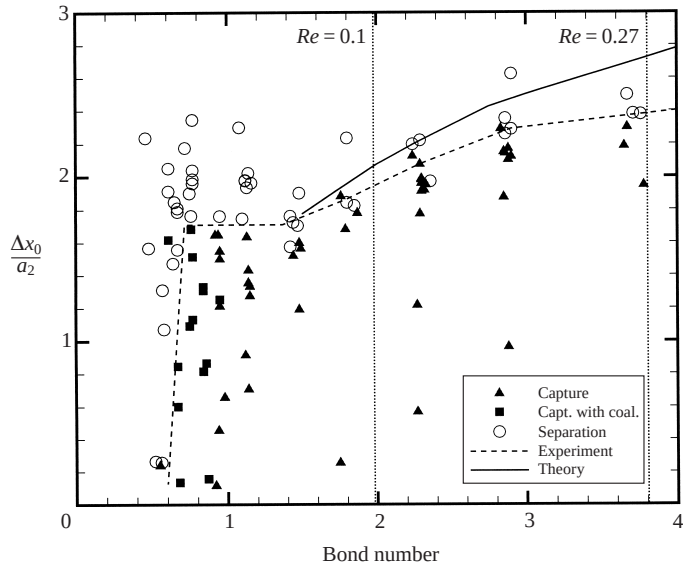

FIGURE 10. As figure 9 but for $\hat{\mu} = 0.002$ and $k = 0.8$.

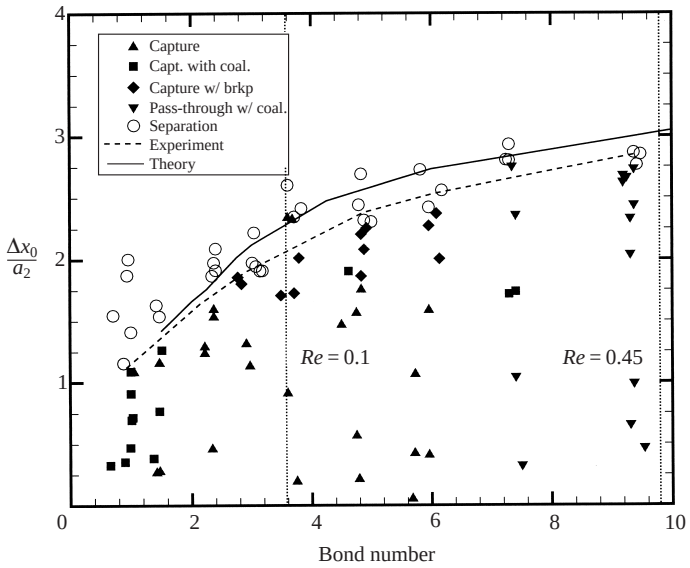

FIGURE 11. As figure 9 but for $\hat{\mu} = 0.1$ and $k = 0.8$. Filled symbols represent capture and pass-through events.

surfactant contamination in System 1. However, an interesting feature of figures 9 and 10 is that the theoretical and experimental critical capture offsets match well for both size ratios ($k = 0.7$ and 0.8). We suspect that the good agreement is due to surfactants being swept to the tails of the drops early in runs where capture occurs, so that their effect is minimal.

Breakup and pass-through

In figure 11, for System 2 with $\hat{\mu} = 0.1$ and $k = 0.8$, breakup with capture and pass-through are indicated, in addition to simple capture. In the pass-through behaviour at

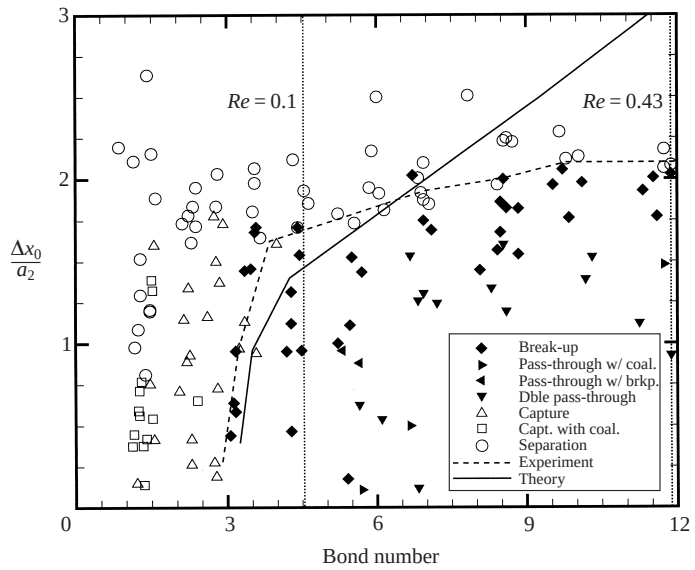

FIGURE 12. As figure 9 but for $\hat{\mu} = 1$ and $k = 0.8$. Filled symbols represent breakup and pass-through events, while hollow ones are for capture and separation without breakup.

$\hat{\mu} = 0.1$, however, coalescence occurs rather than the leap-frog cycling of figure 8. The solid line, based on the simulations of Zinchenko *et al.* (1999), again demonstrates good agreement between theory and experiment. As seen before, capture occurs when the initial horizontal offset is below a critical value that increases with Bo, and the critical offset for capture of very deformable drops and bubbles can be much greater than that for even non-interacting fluid particles. Simultaneous breakup of the smaller drop can also occur, as predicted in the previous simulations (Zinchenko *et al.* 1999), for moderate Bo and offsets just below critical. For System 2, it was difficult to discern whether a small amount of breakup or tip-streaming took place. Evidence of the absence of surfactants for System 2 is the excellent agreement in the isolated drop velocities between theory and experiment (figure 2) and the good agreement in critical offsets (figure 11) over the entire range of Bond numbers. For these reasons, in figure 11, we have labelled questionable runs 'capture with breakup', rather than 'capture with tip-streaming'.

Pass-through ending in coalescence was observed at large Bo for highly deformable drops, whereas coalescence without pass-through was observed at small Bo for less deformable drops. Unlike in the previous two interaction maps, a sharp decline in the critical offset curve and a critical Bond number below which no capture occurred are not observed. Due to the small size of the drops relative to the tank dimensions, it was only possible to obtain results down to $Bo = 0.7$ with the present apparatus. A smaller tank or better optics might be able to provide results in the extremely low Bond number region, which would result in bounding the capture with coalescence region.

A map for System 3 with $\hat{\mu} = 1$ and $k = 0.8$ is shown in figure 12. In the theoretical analysis of Zinchenko *et al.* (1999), critical offset values were calculated for the transition between breakup and separation interactions, and the results are shown as the solid line. In this figure, the closed symbols are for experiments in which breakup of the smaller drop occurred (including pass-through, which was always accompanied by stretching and breaking of the tail of the smaller drop), whereas the open symbols

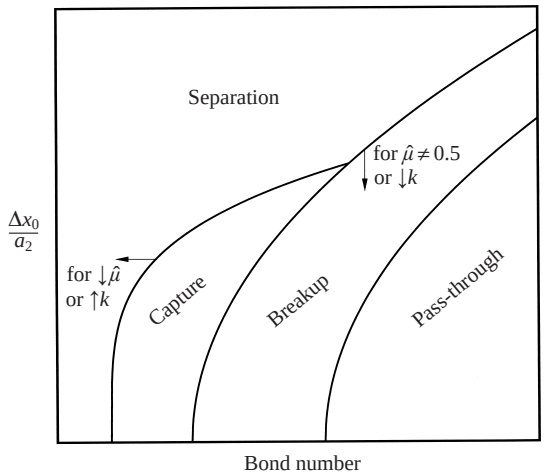

FIGURE 13. A schematic interaction map illustrating the characteristic behaviours observed in the experiments and their dependence on viscosity ratio $\hat{\mu}$ and size ratio k.

are for either separation or capture without breakup. Simple breakup was observed for moderate Bo and initial horizontal offsets just below the critical value, whereas pass-through with breakup was observed for larger Bo and smaller initial offsets. For $Bo < 3$, the smaller drop did not deform enough to break. There is again good agreement between the theoretical predictions and the experimental results, except that they begin to diverge for $Bo > 9$, which may be due to wall or inertial effects.

In the theoretical analysis, it was assumed that, for $Bo < 3$, where the critical offset curve between breakup and separation ends, the only interaction that would be observed is the separation interaction (Zinchenko *et al.* 1999). From the experimental findings, it is clearly seen that this is not the case, as defined regions for capture with and without coalescence exist for $Bo < 3$ in which deformation enhances coalescence beyond spherical drop limitations. The simulations were also not able to predict the pass-through interactions, which were observed for $Bo > 5$. In this map, several variations of the pass-through interaction were observed: cyclic or double pass-through (also called leap-frogging), pass-through followed by complete breakup and separation of the smaller drop, and pass-through followed by coalescence. The distinction between the cyclic pass-through interaction and pass-through followed by separation or coalescence depends on the tank height, as all cyclic pass-through interactions, in an infinitely deep tank, will end either in separation of the broken smaller drop from the leading larger drop, or coalescence of the primary smaller drop with the larger drop.

It is also noted that the mechanisms for capture with coalescence found at the intermediate and large Bond numbers are significantly different from that at small Bond numbers. For small Bo, the smaller drop is entrained behind the larger drop with relatively small deformation (e.g. see figure 6) and there is a significant time delay before coalescence occurs since the castor oil film must drain from the film between the drops. For larger Bo, the deformation is much greater and the smaller drop becomes enveloped within the large dimple or plume which forms at the rear of the larger drop without the smaller drop being sucked through. This arrangement results in the eventual coalescence of the two drops and the inclusion of a small drop of castor oil inside the now single glycerol–water drop. In figure 11, coalescence with

inclusion of a castor oil droplet was observed in three runs indicated by filled square symbols at $Bo = 4.62$, 7.30, and 7.41. All other capture events leading to coalescence in figure 11 occurred at Bond numbers of 1.5 or less and without entrainment of any castor oil. This distinction between the two coalescence mechanisms is similar to nose capture and rim capture predicted by Yiantsios & Davis (1991).

A final, semi-quantitative map is presented as figure 13 showing the boundaries between separation, capture, breakup and pass-through. General trends, based on viscosity ratio and size ratio, are indicated by arrows. Capture, breakup and pass-through all strongly depend on size ratio, so that as k increases, the critical Bond number at which the various phenomena occur decreases. As described in Davis (1999), at $\hat{\mu} \approx 0.5$, the critical Bond number for breakup is a minimum. As the viscosity ratio increases or decreases, the effect of breakup becomes less significant. At very small viscosity ratios, no breakup or pass-through takes place and capture is a predominant interaction.

4. Concluding remarks

Experiments on buoyancy-driven interactions of two glycerol–water drops in castor oil were conducted at low Reynolds numbers to compare with results from boundary-integral calculations. At small drop-to-medium viscosity ratios and moderate to large Bond numbers, drop capture and possible coalescence were observed, in agreement with theory. In addition, at $O(1)$ viscosity ratios, drop breakup was seen, similar to results from simulations. At higher Bo, some discrepancy was observed, with theory overpredicting critical horizontal offsets for capture and breakup, possibly due to wall effects and inertial effects with increasing drop size. At moderate viscosity ratios and moderate to large Bond numbers, new pass-through phenomena were recorded in which the leading drop formed a torus and the smaller drop passed through its centre, sometimes in multiple cycles reminiscent of leap-frogging.

This work was supported by the National Aeronautics and Space Agency, the US Department of Education's GAANN Program, and the NSF-REU Program at the University of Colorado. The authors are grateful to Dr A. Z. Zinchenko for advice on the boundary-integral calculations, and to the late Uwe Schaflinger for providing an advance copy of the paper by Machu *et al.* (2001).

REFERENCES

Ambwani, D. S. & Fort, T. 1979 Pendant drop technique for measuring liquid boundary tensions. In *Surface and Colloid Science, Vol. 11. Experimental Methods* (ed. R. J. Good & R. R. Stromberg). Plenum Press.

Ashgriz, N. & Poo, J. Y. 1990 Coalescence and separation in binary collisions of liquid droplets. *J. Fluid Mech.* **221**, 183–204.

Baumann, N., Joseph, D. D., Mohr, P. & Renardy, Y. 1992 Vortex rings of one fluid in another in free fall. *Phys. Fluids* **4**, 567–580.

de Bruijn, R. A. 1993 Tipstreaming of drops in simple shear flows. *Chem. Engng Sci.* **48**, 277–284.

Cristini, V., Blawzdziewicz, J. & Loewenberg, M. 1998 Drop breakup in three-dimensional viscous flows. *Phys. Fluids* **10**, 1781–1783.

Davis, R. H. 1999 Buoyancy–driven viscous interaction of a rising drop with a smaller trailing drop. *Phys. Fluids* **11**, 1016–1028.

Davis, R. H., Schonberg, J. A. & Rallison, J. M. 1989 The lubrication force between two viscous drops. *Phys. Fluids* **1**, 77–81.

Durlofsky, L., Brady, J. F. & Bossis, G. 1987 Dynamic simulation of hydrodynamically interacting particles. *J. Fluid Mech.* **180**, 21–49.

Faber, T. E. 1995 *Fluid Dynamics for Physicists*. Cambridge University Press.

Guido, S. & Simeone, M. 1998 Binary collision of drops in simple shear flow by computer-assisted video optical microscopy. *J. Fluid Mech.* **357**, 1–20.

Hocking, L. M. 1964 The behaviour of clusters of spheres falling in a viscous fluid. Part 2. Slow motion theory. *J. Fluid Mech.* **20**, 129–139.

Hu, Y. T., Pine, D. J. & Leal, L. G. 2000 Drop deformation, breakup, and coalescence with compatibilizer. *Phys. Fluids* **12**, 484–489.

Joseph, D. D. & Renardy, Y. Y. 1993 *Fundamentals of Two-Fluid Dynamics*. Springer.

Koh, C. J. & Leal, L. G. 1989 The stability of drop shapes for translation at zero Reynolds number through a quiescent fluid. *Phys. Fluids* A **1**, 1309–1313.

Kojima, M., Hinch, E. J. & Acrivos, A. 1984 The formation and expansion of a toroidal drop moving in a viscous fluid. *Phys. Fluids* **27**, 19–32.

Machu, G., Meile, W., Nitsche, L. C. & Schaflinger, U. 2001 Coalescence, torus formation and breakup of sedimenting drops: experiments and computer simulations. *J. Fluid Mech.* (submitted).

Manga, M. & Stone, H. A. 1993 Buoyancy-driven interactions between two deformable viscous drops. *J. Fluid Mech.* **256**, 647–683.

Manga, M. & Stone, H. A. 1995 Collective hydrodynamics of deformable drops and bubbles in dilute low Reynolds number suspensions. *J. Fluid Mech.* **300**, 231–263.

Mellan, I. 1970 *Industrial Solvents Handbook*. Noyes Data Corporation.

Menchaca-Rocha, A., Huidobro, F., Martinez-Davalos, A., Michaelian, K., Perez, A., Rodriguez, V. & Carjan, N. 1997 Coalescence and fragmentation of colliding mercury drops. *J. Fluid Mech.* **346**, 291–318.

Nallani, M. & Subramanian, R. S. 1993 Migration of methanol drops in a vertical temperature gradient in a silicone oil. *J. Colloid Interface Sci.* **157**, 24–31.

Orme, M. 1997 Experiments on droplet collisions, bounce, coalescence and disruption. *Prog. Energy Combust. Sci.* **23**, 65–78.

Pozrikidis, C. 1990 The instability of a moving viscous drop. *J. Fluid Mech.* **210**, 1–21.

Qian, J. & Law, C. K. 1997 Regimes of coalescence and separation in droplet collision. *J. Fluid Mech.* **331**, 59–80.

Sherwood, J. D. 1984 Tip streaming from slender drops in a non–linear extensional flow. *J. Fluid Mech.* **144**, 281–295.

Tretheway, D. C., Muraoka, M. & Leal, L. G. 1999 Experimental trajectories of two drops in planar extensional flow. *Phys. Fluids* **11**, 971–981.

Wei, H. & Subramanian, R. S. 1994 Interactions between two bubbles under isothermal conditions and in a downward temperature gradient. *Phys. Fluids* **6**, 2971–2978.

Yamada, H. & Matsui, T. 1978 Preliminary study of mutual slip-through of a pair of vortices. *Phys. Fluids* **21**, 292–294.

Yamada, H. & Matsui, T. 1979 Mutual slip-through of a pair of vortex rings. *Phys. Fluids* **22**, 1245–1249.

Yiantsios, S. G. & Davis, R. H. 1990 On the buoyancy-driven motion of a drop towards a rigid surface or a deformable interface. *J. Fluid Mech.* **217**, 547–573.

Yiantsios, S. G. & Davis, R. H. 1991 Close approach and deformation of two viscous drops due to gravity and van der Waals forces. *J. Colloid Interface Sci.* **144**, 412–433.

Zhang, X. & Davis, R. H. 1991 The rate of collisions of small drops due to Brownian or gravitational motion. *J. Fluid Mech.* **230**, 479–504.

Zhang, X., Davis, R. H. & Ruth, M. F. 1993 Experimental study of two interacting drops in an immiscible fluid. *J. Fluid Mech.* **249**, 227–239.

Zinchenko, A. Z. 1982 Calculations of the effectiveness of gravitational coagulation of drops with allowance for internal circulation. *Prikl. Mat. Mech.* **46**, 58–65.

Zinchenko, A. Z., Rother, M. A. & Davis, R. H. 1997 A novel boundary–integral algorithm for viscous interaction of deformable drops. *Phys. Fluids* **9**, 1493–1511.

Zinchenko, A. Z., Rother, M. A. & Davis, R. H. 1999 Cusping, capture, and breakup of interacting drops by a curvatureless boundary-integral algorithm. *J. Fluid Mech.* **391**, 249–292.